Applied Composite Materials, 0():xxx-xxx, 2014.

Identification of Fracture Toughness for Discrete Damage Mechanics Analysis of Glass-Epoxy Laminates

E. J. Barbero[1] and F. A. Cosso [2]
Mechanical and Aerospace Engineering, West Virginia University,
Morgantown, WV 26506-6106, USA
and
X. Martinez [3]
Technical Univeristy of Catalonia (UPC), Spain

Abstract

A methodology for determination of the intralaminar fracture toughness is presented, based on fitting discrete damage mechanics (DDM) model predictions to available experimental data. DDM is constitutive model that, when incorporated into commercial finite element software via user material subroutines, is able to predict intralaminar transverse and shear damage initiation and evolution in terms of the fracture toughness of the composite. The applicability of the DDM model is studied by comparison to available experimental data for Glass-Epoxy laminates. Sensitivity of the DDM model to h- and p-refinement is studied. Also, the effect of in-situ correction of strength is highlighted.

Keywords

A. Polymer-matrix composites (PMCs); B. Transverse cracking; C. Damage mechanics; C. Finite element analysis (FEA); Parameter Identification.

1 Introduction

Prediction of damage initiation and accumulation in polymer matrix, laminated composites is of great interest for the design, production, certification, and monitoring of an increasingly large variety of structures. Matrix cracking due to transverse tensile and shear deformations is normally the first mode of damage and, if left unmitigated often leads to other modes such as delamination, fiber failure of adjacent laminas due to load redistribution, and reduction of the shear stiffness, which in turn deteriorates the longitudinal compressive strength of the composite [1]. Furthermore, matrix

[1]Corresponding author. The final publication is available at http://dx.doi.org/10.1007/s10443-013-9359-y
[2]Graduate Research Assistant.
[3]Professor (UPC) and Researcher (CIMNE)

cracking leads to increased permeability and exposes the fibers to deleterious environmental attack, which in the case of Glass and polymeric fibers, may lead to unacceptable material degradation.

As any other fracture process, transverse matrix cracking is defined by failure onset and propagation. The simplest way to address matrix cracking is by limiting the design allowable to the material strength at failure onset. Many models follow this approach [2, 3]. Most of them address transverse matrix cracking together with other failure mechanisms such as matrix compressive failure, fibre tensile rupture or fibre compression failure. These models can be included in a finite element code using the ply discount method [4, § 7.3.1].

More sophisticated models are capable of predicting damage onset and propagation. In [5–7], the response of each lamina is obtained from a meso-model that couples the behaviour of a single layer and an interlaminar layer. The first layer uses a damage model capable of differentiating between tensile and compression loads, thus accounting for transverse matrix crack effects. The second layer uses a two dimensional damage model that only takes into account stresses that lead to delamination failure. Parameter identification is described in [6, 7] and validation with open-hole tensile tests on quasi-isotropic laminates is given in [8].

Another approach to simulate the onset and propagation of transverse matrix cracking, as well as other failure mechanisms, is serial-parallel mixing theory [9]. This formulation obtains the composite response from the constitutive performance of its constituents, usually matrix and fibre, each one of them simulated with its own constitutive law. With this theory it is possible to use any given non-linear material model, such as damage or plasticity, to characterize the composite components. The correct determination of failure onset and propagation depends on the capacity and accuracy of the model used. Examples of of this formulation are shown in [10–12].

When looking into the models developed specifically to address the phenomenon of transverse matrix cracking, most of them establish a relation between the available strain energy of the material and the density of matrix cracks [13–23]. Following this approach, [17, 19] uses finite fracture mechanics to obtain the energy release rate required to double the crack density, with the apparition of a new crack between two existing cracks. This model was improved with the concept of incremental and continuous variation of crack density [20], showing that the calculation of the energy release rate required to crack propagation is more accurate if crack density is assumed to grow continuously, instead of doubling at each increment. Further, the equivalent constrained model (ECM) [21, 22], defines a law that provides the evolution of stiffness as matrix crack density increases. Again, the increment of matrix cracks depends on the strain energy release rate.

Some of the above mentioned formulations provide analytical expressions that can be used to obtain the mechanical response for simple geometry and load configurations. However, it is often necessary to include the constitutive model into Finite Element Analysis Software. Some models have been included in commercial FEM software [24–26], others that are available as plugins for existing FEA software [27, 28], or as user programmable features, including UMAT, UGENS [29] or USERMAT [30].

In this manuscript, it is proposed to use Discrete Damage Mechanics (DDM) for the simulation of transverse matrix cracking. Briefly, DDM [31] is a constitutive model that is objective [32], i.e., the predictions are not affected by the element size or type (linear, quadratic, etc.). Furthermore, only two material parameters, the fracture toughness in modes I and II, are required to predict both initiation and evolution of transverse and shear damage.

Since fracture toughness is used to predict damage initiation (transverse and shear strengths are not used) DDM does not require in-situ correction of strength. No hardening/softening parameters are required either, which avoids costly experimentation that would otherwise be required to determine them. Also, as it is shown in this work, DDM parameters can be identified for Glass fiber composites. This is not easily done with continuum damage mechanics (CDM) models because

their state variables (damage variables), are not direclty measurable [33]. As a result, CDM's material parameters must be identified using a macroscopic effect, such as the loss of stiffness, which in most cases is difficult to measure [34].

Finally, DDM has also the advantage that it is already available to be used in commercial FEA environments such as Abaqus[4] [26] and ANSYS/Mechanical[5] [35], in the form of UMAT, UGENS [29], and USERMAT [30]. It is also possible to obtain the composite response to uniaxial tensile loads with the webpage application [36, `Cadec/Chapters/Damage/DDM`].

The objective of this manuscript is to propose a methodology to identify the fracture toughness using available experimental data. Once the DDM model parameters are identified, validation is presented by predicting other, independent results, and conclusions are drawn about the applicability of the model.

Standards exist for measuring interlaminar (not intralaminar) fracture toughness in mode I (ASTM D5528) and proposed methods exists for mode II [37, 38], but no standard test method exist to measure intralaminar fracture toughness. Thus, a method to identify the DDM model parameters is necessary.

2 Discrete Damage Mechanics

Given the crack density λ and the shell strain ϵ, κ, DDM updates the state variable, i.e., the crack density, and calculates the shell stress resultants N, M, and tangent stiffness matrix A_T, B_T, D_T, all of them functions of crack density. The crack density λ is an array containing the crack density for all laminas at an integration point of the shell element. Since the strain is conjugate to the shell stress resultant, DDM provides a constitutive model that can be implemented as a user material subroutine (UMAT, VUMAT, USERMAT) [30, usermatps-901] for flat plane stress elements and as a user general section (UGENS) for curved shell elements [29, ugens-std].

2.1 Description of the Model

In DDM, damage initiation and evolution are controlled by a single equation representing the Griffith's criterion for an intralaminar crack, i.e., the undamaging domain is defined by

$$g(\epsilon, \lambda) = max\left[\frac{G_I(\epsilon,\lambda)}{G_{IC}}, \frac{G_{II}(\epsilon,\lambda)}{G_{IIC}}\right] - 1 \leq 0 \tag{1}$$

where G_I, G_{II} are the strain energy release rates (ERR) in modes I and II, calculated with (14)-(15), and G_{IC}, G_{IIC} are the invariant material properties representing the energy necessary to create a new crack. We shall see that for fixed strain, both are decreasing functions of λ and thus (1) exhibits strain-hardening for increasing λ, resulting in stress-softening as a function of strain.

DDM calculates G_I, G_{II} solving the 3D equilibrium equations in the RVE (Fig. 1)

$$\nabla \cdot \sigma - f = 0 \tag{2}$$

reduced to 2D by the following approximations. The u_3 component of displacement is eliminated by assuming a state of plane stress for symmetric laminates under membrane loads,

$$\sigma_3 = 0 \quad ; \quad \frac{\partial u_3}{\partial x_i} = 0 \quad with \quad i = 1, 2 \tag{3}$$

[4] Abaqus and Simulia are trademarks or registered trademarks of Dassault Systèmes or its subsidiaries in the United States and/or other countries.

[5] Ansys® is a registered trademark of ANSYS Inc.

Then, (2) are written in terms of the average of the displacements over the thickness of each lamina, defined as

$$\hat{u}_i^{(k)} = \int_{-t_k/2}^{t_k/2} u_i(z)dz \tag{4}$$

where t_k is the thickness of lamina k. Next, the intralaminar shear stress is assumed to be linear in each lamina k, from the interface between laminas $k-1$ and k (denoted $k-1,k$) to the interface between laminas k and $k+1$,

$$\tau_{j3}^{(k)}(x_3) = \tau_{j3}^{k-1,k} + \left(\tau_{j3}^{k,k+1} - \tau_{j3}^{k-1,k}\right) \frac{x_3 - x_3^{k-1,k}}{t_k} \quad ; \quad j = 1,2 \tag{5}$$

where x_3 is the coordinate along the thickness of the laminate, and $x_3^{k-1,k}$ is the coordinate of the interface between laminas $k-1$ and k. Therefore, the 3D equilibrium equations (2) reduce to a system of 2N partial differential equations (PDE) in two dimensions, in terms of average displacements, with two equations per lamina.

Periodically spaced cracks, which propagate suddenly in a unstable fashion through the thickness of the lamina and along the fiber direction are assumed [39], [4, § 7.2.1]. Therefore, a representative volume element (RVE) is chosen spanning the laminate thickness between two adjacent cracks (Fig. 1). The crack density is inversely proportional to the length $2l$ of the RVE,

$$\lambda = 1/2l \tag{6}$$

Thus, crack density is represented in the model by the length of the RVE. Since the RVE is independent of the finite element discretization, and the constitutive model is formulated in terms of displacements (not strains), the constitutive model is objective, without needing a characteristic length. By plotting the reaction force vs. applied displacement on the boundary, the numerical results presented in this work corroborate the objectivity of the model.

The PDE system is complemented by the following boundary conditions. The surface of the cracks in lamina c, located at $x = \pm l$, are free boundaries, and thus subject to zero stress

$$\int_{-1/2}^{1/2} \hat{\sigma}_j^{(c)}(x_1, l)\, \mathrm{d}x_1 = 0 \quad ; \quad j = 2,6 \tag{7}$$

All laminas $m = 1..N$ with $m \neq c$, that is, excluding the cracking lamina c, undergo the same displacement at the boundaries $(-l, l)$ when subjected to a membrane state of strain. Taking an arbitrary lamina $r \neq c$ as a reference, the other displacements are

$$\hat{u}_j^{(m)}(x_1, \pm l) = \hat{u}_j^{(r)}(x_1, \pm l) \quad ; \quad \forall m \neq k \quad ; \quad j = 1,2 \tag{8}$$

Finally, the stress resultant from the internal stress equilibrates the applied load. In the direction parallel to the surface of the cracks (fiber direction x_1) the load is supported by all the laminas in the laminate,

$$\frac{1}{2l} \sum_{k=1}^{N} t_k \int_{-l}^{l} \hat{\sigma}_1^{(k)}(1/2, x_2) dx_2 = N_1 \tag{9}$$

but, in the direction normal to the crack surface (x_2 direction), only the intact laminas $m \neq c$ carry loads (normal and shear)

$$\sum_{m \neq k} t_m \int_{1/2}^{1/2} \hat{\sigma}_j^{(m)}(x_1, l)\, dx_1 = N_j \quad ; \quad j = 2, 6 \tag{10}$$

The solution of the PDE system results in finding the displacements in all laminas $\hat{u}_i^{(k)}$, and by differentiation, the strains in all laminas. Next, the compliance S of the laminate is calculated by solving three load cases

$${}^{a}N/t = \left\{ \begin{array}{c} 1 \\ 0 \\ 0 \end{array} \right\}; \quad {}^{b}N/t = \left\{ \begin{array}{c} 0 \\ 1 \\ 0 \end{array} \right\}; \quad {}^{c}N/t = \left\{ \begin{array}{c} 0 \\ 0 \\ 1 \end{array} \right\}; \quad \Delta\, T = 0 \tag{11}$$

where t is the thickness of the laminate. Since the three applied stress states are unit values, for each case, *a, b, c,* the volume average of the strain represents one column in the laminate compliance matrix

$$S = \begin{bmatrix} {}^{a}\epsilon_x & {}^{b}\epsilon_x & {}^{c}\epsilon_x \\ {}^{a}\epsilon_y & {}^{b}\epsilon_y & {}^{c}\epsilon_y \\ {}^{a}\gamma_{xy} & {}^{b}\gamma_{xy} & {}^{c}\gamma_{xy} \end{bmatrix} \tag{12}$$

Next, the laminate inplane stiffness $Q = A/t$ in the coordinate system of lamina k is

$$Q = S^{-1} \tag{13}$$

The degraded CTE of the laminate $\{\alpha_x, \alpha_y, \alpha_{xy}\}^T$ are given by the values $\{\epsilon_x, \epsilon_y, \gamma_{xy}\}^T$ obtained for the case with loading $N = \{0, 0, 0\}^T$ and $\Delta T = 1$. Then, the ERR in fracture modes I and II are calculated as follows [40, 41, (9.36)-(9.37)]

$$G_I = -\frac{V_{RVE}}{2\Delta A} \left(\epsilon_2 - \alpha_2 \Delta T\right) \Delta Q_{2j} \left(\epsilon_j - \alpha_j \Delta T\right) \quad ; \quad \text{opening mode} \tag{14}$$

$$G_{II} = -\frac{V_{RVE}}{2\Delta A} \left(\epsilon_6 - \alpha_6 \Delta T\right) \Delta Q_{6j} \left(\epsilon_j - \alpha_j \Delta T\right) \quad ; \quad \text{shear mode} \tag{15}$$

Tearing mode III does not occur because out of plane displacements of the lips of the crack are constrained by the adjacent laminas in the laminate. The crack density is treated as a continuous function, as suggested in [20], rather than a discrete function. Thus, the crack density is found using a return mapping algorithm (RMA) to satisfy $g = 0$ in (1), as follows

$$\Delta\lambda_k = -g_k / \frac{\partial g_k}{\partial \lambda} \tag{16}$$

2.2 Stress Softening

The ERR that would be released by the laminate if a potential crack would appear, increases with strain according to (14), as it is shown in Fig. 2, but the crack does not materialize until the available ERR exceeds the critical value. At this point a crack appears and dissipation takes place. The ERR continues to grow after the critical value, meaning that new cracks appear, but the

ERR grows at a slower rate than in the undamaging domain because the stiffness of the material decreases with damage.

The RMA (16) finds the value of crack density λ that takes the damage activation function to $g = 0$ as per (1). The search is done at constant strain, inside the DDM constitutive model for a given iteration of the structural analysis program (e.g., Abaqus, ANSYS, etc.).

An increase of crack density produces a drop of stiffness, thus a drop of ERR as per (14)-(15). As a result, once the crack density that satisfies $g = 0$ is found, no more damage can take place unless the strain grows, which only can be imposed by the structural analysis program in a subsequent iteration. This means that (14)-(15) displays strain hardening. To illustrate this, consider (14) for mode I. With reference to the dimensions of the RVE in Fig. 1, we have that $V_{RVE} = 2l \times 1 \times t$. For each new crack, the crack area grows by $\Delta A = t_k \times 1$ and the crack density doubles, so that $\Delta\lambda = \lambda$. Finally, considering (6), and for a case of uniaxial state of stress in a tensile test, we have

$$G_I = \left(-\frac{t}{t_k}\frac{\Delta E}{2\Delta\lambda}\right)\epsilon^2 \tag{17}$$

where $E(\lambda)$ is the laminate modulus in the direction of the applied strain ϵ. At constant strain, a decreasing parenthesis in (17) assures that once the RMA has converged to a value of λ, no more damage can occur without an increase of strain. Variation of G_I/ϵ^2 vs. crack density is shown in Fig. 3. Unlike other damage models in the literature, the DDM constitutive model *calculates* the strain hardening (stress softening). Therefore, it is not necessary to *postulate* a hardening/softening law, and more importantly, it is not necessary to perform costly experiments to calibrate it. Instead, the hardening/softening law is *provided* by the DDM formulation.

Modulus degradation of the cracking lamina is shown in Figs. 4–7. Once the degraded stiffness of the laminate (13) is known, the degraded stiffness of the cracked lamina, i.e., lamina c, can be computed as

$$Q^{(c)} = \frac{t}{t_c}\left[Q - \sum_{m=1}^{n}(1-\delta_{mc})Q^{(m)}\frac{t_m}{t}\right] \tag{18}$$

and from it, the the stress carried by the cracking lamina is calculated and shown in Figs. 8–9. Stress softening occurs immediately after damage initiation, as shown in Figs. 8–9, but unlike PDA [26, § 24.3], the remaining stress in the cracking lamina does not drop to zero. In fact, for laminates 3, 4, 5, the stress in the cracking lamina grows after the initial reduction. This means that the stiffness of the cracking lamina does not decrease as rapidly as the increasing strain applied to it. Note that laminates 3–5 have compliant support layers at $\pm\theta = 15, 30, 40°$. The more compliant the supporting layer is, the higher the stress taken by the cracked lamina.

Since DDM is insensitive to element size (see Section 5), Fig. 8 could be plotted in terms of a displacement δ obtained for example by multiplying the strain by a characteristic length. In Abaqus PDA, a characteristic length l_c is chosen as the square root of the area of each element in the mesh, $\delta = l_c\epsilon$ [26], but DDM does not require the use of a characteristic length to achieve objectivity.

A striking difference is noted comparing Fig. 8 with [34, Fig. 1] because the softening law in Abaqus PDA [26, § 24.3] ($\sigma-\delta$ plot), assumes a linear decrease of σ after crack initiation, eventually dropping to zero stress. Such empirical softening law contradicts Figs. 8–9. Although Figs. 8–9 are the result of a model prediction, the model is validated for these same laminates by comparing to experimental data in the form of both crack density vs. strain (laminate 1) and modulus reduction vs. strain (laminates 2–5). Since the model calculates the stress σ_2 in the cracking lamina using the predicted modulus reduction, and the latter is validated, one can safely conclude that the calculated stress is correct.

3 Strength Criterion

The dimensions of the specimens used in the experiments reported in the literature are 12 mm wide with a free length of 110 mm. The material is Fiberite/HyE 9082Af with ply thickness $t_k = 0.144$ mm [42] with a literature reported value $F_{2t} = 40$ MPa [43]. All laminates were subjected to axial deformation ε_x along the length of the specimen. None of the laminas in these laminates is subjected to fiber modes or matrix compression. The 90° laminas in laminates 1–5 in Table 1 are subjected to pure traction and no shear, so damage initiation is controlled by the parameter F_{2t} when a strength criterion is used and by G_{IC} when a fracture criterion is used. The $\pm\theta^\circ$ laminas in laminates 6–7 in Table 1 are subjected to a combination of traction and shear, so damage initiation involves the parameters F_{2t}, F_6 when a strength criterion is used, and G_{IC}, G_{IIC} when a fracture criterion is used. Seven laminates are considered in Tables 1–2. The laminate thickness is calculated in terms of the laminate stacking sequence (LSS, column 2 in Table 1) and the ply thickness. The laminate modulus in the load direction E_x is calculated using an online laminate analysis software [36] and unidirectional lamina properties summarized in [34, Table 2]. The strain ϵ at first ply failure (FPF) is read from the figures in the source articles [42,44]. At this point, the experimental FPF load per unit width is computed as

$$FPF_{exp} = t\ E_x\ \epsilon_{FPF} \tag{19}$$

The transverse and shear strengths of the unidirectional lamina reported in the literature are not reliable because large scatter in the experimental data. Furthermore, since they are not invariant material properties, they have to be corrected for in-situ effect [4, § 7.2.1, (7.42)]. The correction is implemented in [36] as

$$\begin{aligned} F_{2t}^{is} &= 1.12\sqrt{\frac{2\ t_t}{t_e}}F_{2t} \\ F_6^{is} &= \sqrt{\frac{2\ t_t}{t_e}}F_6 \\ t_e &= min(t_k, t_t) \end{aligned} \tag{20}$$

where t_k, t_t are the thickness of the ply in question and the transition thickness of the material, respectively. The later is found experimentally as the transition between thin and thick ply behavior [45], which can be taken as $t_t = 0.6, 0.8$ mm for Glass-Epoxy and Carbon-Epoxy, respectively. Besides that, F_{2t}, F_6 are the transverse and shear strengths of the unidirectional lamina, and F_{2t}^{is}, F_6^{is} are the in-situ values for the ply with thickness t_k.

Coincidentally, the FPF calculated with in-situ correction (labeled "FPF in-situ" in Table 2) coincides with the experimental value (labeled FPF exp) for laminate #1, but not for the rest. Meanwhile, the FPF calculated without in-situ correction (labeled FPF CLT) is highly inaccurate for all laminates. The % error between the CLT prediction and the experimental FPF ranges from 58% to 138%, while the prediction corrected by in-situ effect is within 32% with an average error of only 16%. Along with [46] for Carbon-Epoxy, the results discussed in this section represent the first comprehensive validation of equations (20).

Next, the calculated in-situ FPF and experimental values of FPF are used to correct the unidirectional transverse strength F_{2t} for each laminate, as reported in the last column in Table 2. On average, $F_{2t} = 46.38$ MPa, vs. 40.0 MPa reported in [43]. In comparison, the unidirectional transverse strength has been previously identified with Abaqus as $F_{2t} = 48.5725$ MPa for the same material [34, Table 3]. In conclusion, while in-situ correction improves the prediction of damage initiation, the prediction can be further improved by adjusting the value of unidirectional lamina

strength (in this case from 40 to 46.38 MPa) to better match the experimental values of damage initiation.

4 Fracture Mechanics Criterion

The fracture mechanics criterion is given in (1) with the ERRs calculated with (14)–(15). An interacting criterion was used in [31, (27)] but a non interacting criterion (1) is used in this manuscript because the addition of an interacting term does not improve the prediction of observed response for the available experimental data.

Data available from the literature is used in this section either to determine the material properties or to compare predictions with experimental data. One experimental data set, i.e., for $[0/90_8/0_{1/2}]_S$ was used to identify (i.e., determine) the values of the material parameter, namely G_{IC}. This laminate was used because it presents only mode I cracks. The rest of the data sets are used to compare the predictions of the model with experimental data.

All the laminates considered for the study are symmetric and balanced. Therefore a quarter of the specimen was used for the analysis using symmetry boundary conditions and applying a uniform strain via imposed displacements on one end of the specimen. A longitudinal displacement of 1.1 mm was applied to reach a strain of 2%. Abaqus S4R shell elements were used for most of the study but the convergence study also considered quadratic S8R shell elements, as well as ANSYS linear PLANE 181 and quadratic PLANE 281.

DDM is a constitutive model. In that sense, a finite element program such as Abaqus provides the laminate strain $\{\epsilon, \kappa\}$ and DDM returns the laminate stress resultants $\{N, M\}$ that equilibrate the strain $\{\epsilon, \kappa\}$ after the correct degradation of material stiffness has been calculated by DDM. The stiffness degradation is calculated as in (13) for a crack density calculated as in (16) in such a way that (1) is satisfied. In addition, the constitutive model returns the secant and tangent stiffness matrices of the laminate.

While using Abaqus, DDM was implemented as a user general section UGENS. A UGENS subroutine contains all the code to provide Abaqus with the laminate response, including the laminate stress resultants $\{N_x, N_y, N_{xy}, M_x, M_y, M_{xy}\}$, the secant laminate stiffness $[ABD]$, and the tangent laminate stiffness $[A_T, B_T, D_T]$. Abaqus performs all the functions of the structural analysis except for the constitutive response, with the later provided by DDM. For each Gauss point, and at each iteration of the structural analysis, Abaqus provides the laminate strain $\{\epsilon, \kappa\}$ and DDM returns the material response. The UGENS is used with shell elements S4R and S8R.

While using ANSYS, the DDM model was implemented as a user material (USERMAT). A USERMAT subroutine contains all the code to provide ANSYS with the stress $\{\sigma_x, \sigma_y, \sigma_{xy}\}$, the secant stiffness matrix $[C]$, and the tangent stiffness matrix $[C_T]$ of an homogeneous material that is equivalent in response to the laminate. The USERMAT is then used along with elements PLANE 181 or PLANE 281 to model the flat specimen in a state of plane stress and axial extension. Since DDM models a laminate with all of its detail, homogenization is required to obtain the constitutive response of the equivalent, homogeneous material, which is performed as follows. The components of stress are calculated as $\sigma_\alpha = N_\alpha/t$, where $\alpha = x, y, xy$ and $t = \sum_1^N t_k$ is the laminate thickness; N is the number of laminas in the laminate. The stress resultants N_α are calculated by DDM to equilibrate the strain $\{\epsilon_x, \epsilon_y, \gamma_{xy}\}$ supplied by ANSYS once the crack density has converged inside the DDM code. The homogeneization of the secant and tangent constitutive matrices are calculated as $[C] = [A]/t$ and $[C_T] = [A_T]/t$, where $[A]$ is the 3×3 extensional stiffness matrix of the laminate [4, (6.16)], as a function of crack density λ, and t is the thickness of the laminate. Note that in a USERMAT, the bending $[D]$ and bending-extension $[B]$ matrices are ignored. Thus,

the USERMAT can be used only to model plates under membrane loads, while the UGENS can be used to model the combined membrane-flexural behavior of curved shells.

The difference between USERMAT (or UMAT) and UGENS implementation highlights an advantage of DDM over local constitutive models. Most damage constitutive models in the literature are *local*, in the sense that they model the constitutive behavior $\sigma = \sigma(\epsilon, \lambda)$, at a material point inside a lamina (e.g., Simpson integration point inside a lamina), without direct coupling with the damage taking place simultaneously in other laminas. In contrast, DMM takes into account all laminas simultaneously in the RVE (see § 2.1 and Fig. 1). Local models can be implemented using USERMAT (or UMAT) to be used at the lamina level, but in doing so, the local models update the state variables (e.g., crack density) in a given lamina using the values of the state variables for the remaining laminas from a prior iteration of the structural analysis program. On the other hand, DDM needs to calculate the entire laminate at once, thus requiring a UGENS implementation (or the homogenization scheme used for ANSYS USERMAT). Furthermore, the fact that local models $\sigma = \sigma(\epsilon, \lambda)$ implicitly affect the volume around an integration point, causes the solution to be mesh dependent, thus requiring additional steps to attain objectivity [32].

Using the USERMAT/UGENS implementation described above, the value of critical energy release rate G_{IC} was identified in such a way that the DDM model provides a best fit to the experimental crack density λ vs. stress σ_x for laminate 1 in Tables 1–2. The experimental data and the fitted DDM model results are shown in Fig. 10.

The error was calculated using the usual formula

$$Error = \frac{1}{n}\sqrt{\sum_{i=1}^{n}\left[\chi^{model}(\xi_i) - \chi^{experim}(\xi_i)\right]^2} \tag{21}$$

where $\chi^{model}, \chi^{experim}$ are the predicted and experimental values of the dependent variable, respectively; ξ_i is the test progress indicator, be it stress or strain depending on how the experimental data is reported in the literature, and n is the number of experimental data points available. The dependent variables used in this study include crack density λ, laminate modulus E_x, and laminate Poisson's ratio ν_{xy}.

By adjusting the parameters G_{IC}, the minimization algorithm converges to a global minimum. A MATLAB script was executed to look for the minimum error (21), by repeatedly executing Abaqus with parameters varying as per the Simplex method [47]. The converged values of $G_{IC} = 253.5\ J/m2$ was obtained for Fiberite/HyE 9082Af. The best fit can be seen in Fig. 10. The error, i.e., the difference between the prediction and experimental data points, is very small and is due only to the dispersion of the experimental results.

For laminates 1, 6, and 7 [44], the measured property is crack density λ and the independent variable is the applied laminate strain ϵ_x. For laminates 2–5 [42], the independent variable is again strain but the dependent variable is the normalized modulus and the normalized Poisson's ratio.

Predicted crack density vs. applied strain for laminates 6 and 7 are shown in Figs. 11 and 12, respectively; both presenting good agreement between model and the experiments. In both cases, mode I fracture was assumed to be dominant, which is corroborated by the quality of the predictions.

Predicted laminate modulus E_x vs. applied strain for laminates 2–5, are shown in Figs. 4–7. In all cases, both damage onset and evolution are predicted quite well.

Predicted Poisson's ratio ν_{xy} vs. applied strain for laminates 2–5, are shown in Figs. 13–16. In all cases, both damage onset and evolution are predicted quite well.

5 Convergence

In this section we assess the sensitivity of the DDM model to h- and p-refinement, realized by mesh refinement and by changing the element type, respectively. Reaction force vs. applied displacement are reported in Fig. 17 using two discretizations, namely 1 and 100 elements of type S4R in Abaqus, thus demonstrating h-refinement. Furthermore, the analysis is repeated using elements S8R in Abaqus, thus achieving p-refinement.

Since a uniform state of strain is applied, h- and/or p-refinement is not necessary to converge on a solution, unless the constitutive model were mesh dependent (see [34, Figs. 14–15]). Objectivity of the DDM constitutive model is verified by showing that the results are not affected by element size or type, namely linear S4R or quadratic S8R (Fig. 17). Abaqus linear S4R elements were used while adjusting the fracture toughness G_{IC}, but the predictions are not affected if the element is changed to Abaqus quadratic S8R, or ANSYS linear PLANE182 or quadratic PLANE183 elements.

6 Conclusions

A practical methodology is proposed to determine the material parameters, namely the critical ERR using laminate experimental data in the form of crack density vs. strain, then predicting modulus reduction vs. strain. To identify the material parameters, i.e., the critical energy release rate, crack density is preferred to modulus reduction because the reduction of laminate modulus due to transverse matrix damage is typically small, and thus parameter identification is difficult using modulus vs. strain data.

From the model response obtained, it is observed that DDM predictions are good for matrix cracking of Glass-Epoxy laminas, not only those oriented at 90 degrees with respect to the load direction, but also at ± 70 and ± 55 degrees. Also, the model predictions are good when the supporting laminas change from very stiff (0 deg) to very compliant (± 40 degrees).

When using a strength criterion, the need to correct the *lamina* intralaminar strength values by in-situ effect is demonstrated, but in-situ effect is inherently present in Discrete Damage Mechanics, thus not requiring extra steps in the model implementation. Also, it is shown that the cracking laminas do not lose their stiffness completely, with stress softening not reaching zero stress even for very large strains. Damage models other than DDM commonly employ empirical softening equations, which often assume that the stiffness of the damaging lamina vanishes for large strains. This is shown to be incorrect for the materials and laminates included in this study.

Acknowledgements

The financial support provided by NASA EPSCoR grant NNH09ZNE002C is appreciated.

Figures

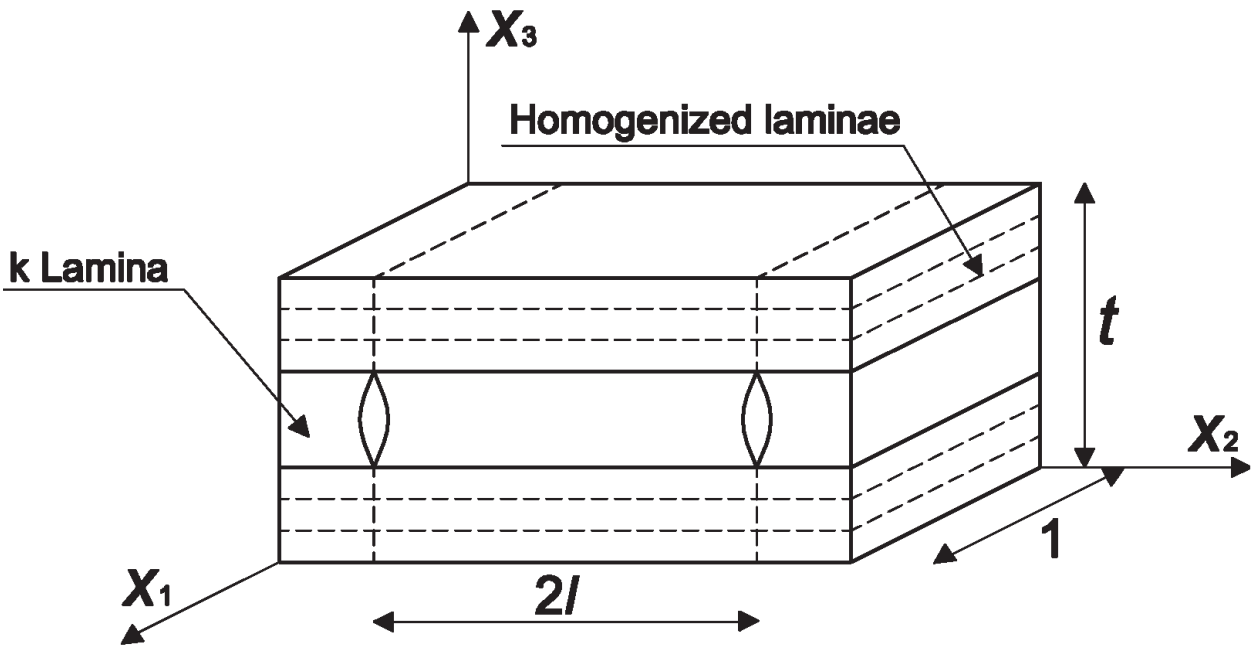

Figure 1: Representative volume element between two adjacent cracks.

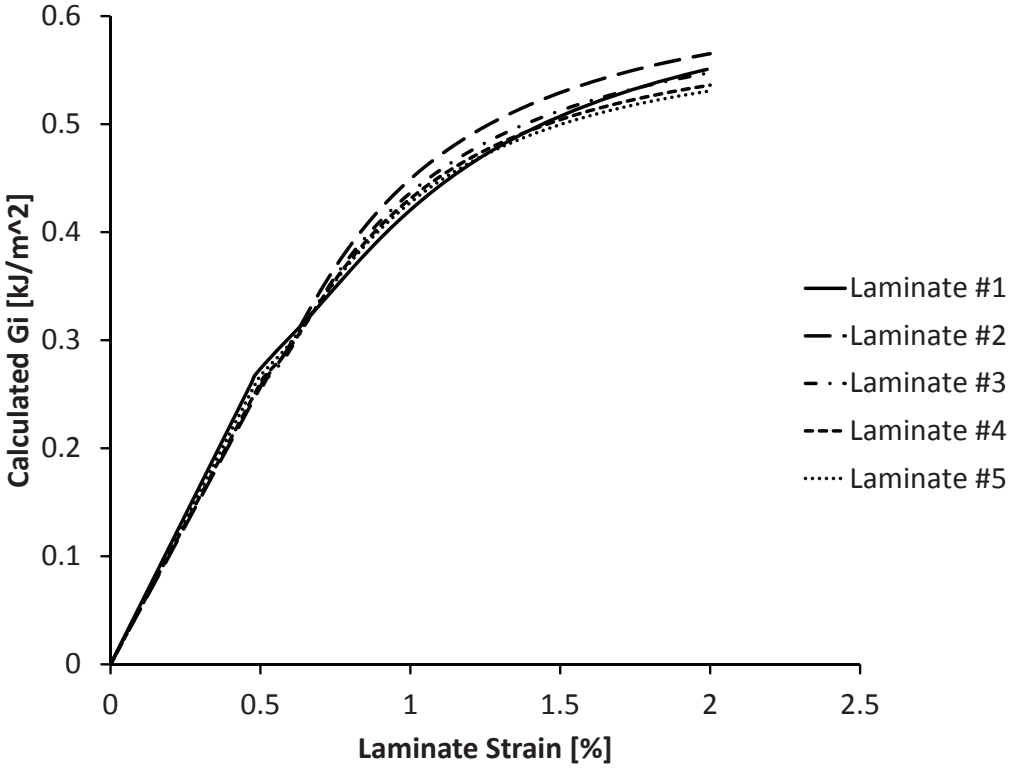

Figure 2: Calculated Energy Release Rate (ERR, G_I) for a crack opening in mode I.

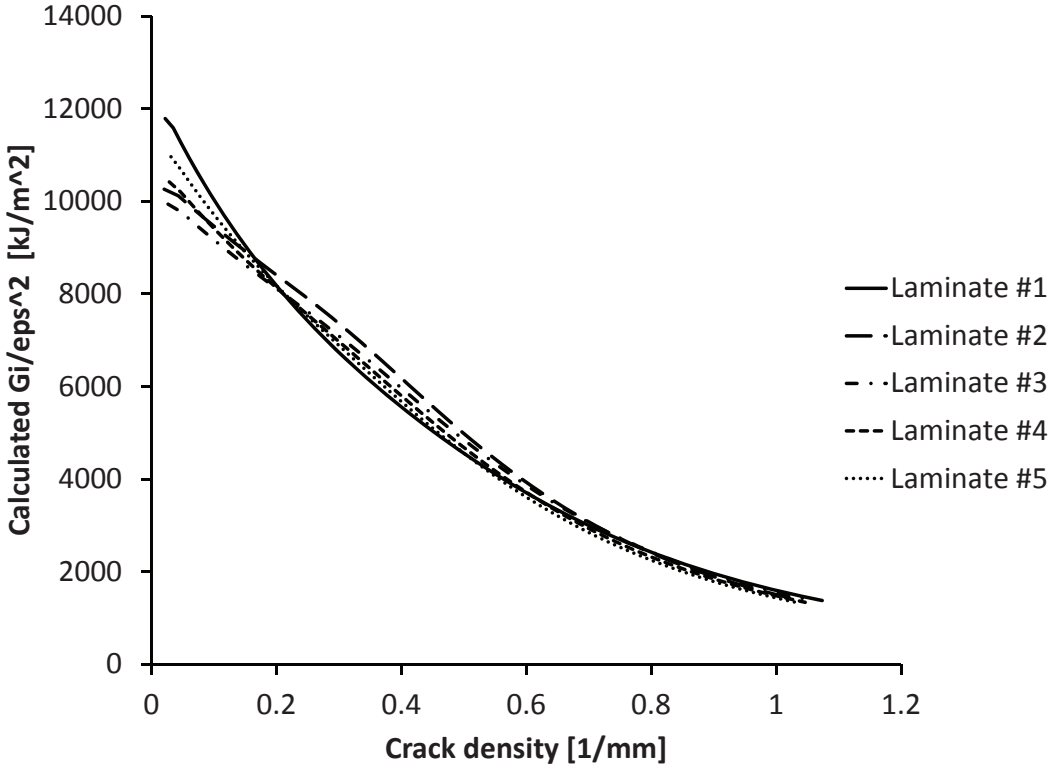

Figure 3: Calculated intrinsic energy release rate G_I/ϵ^2 for a crack opening in mode I.

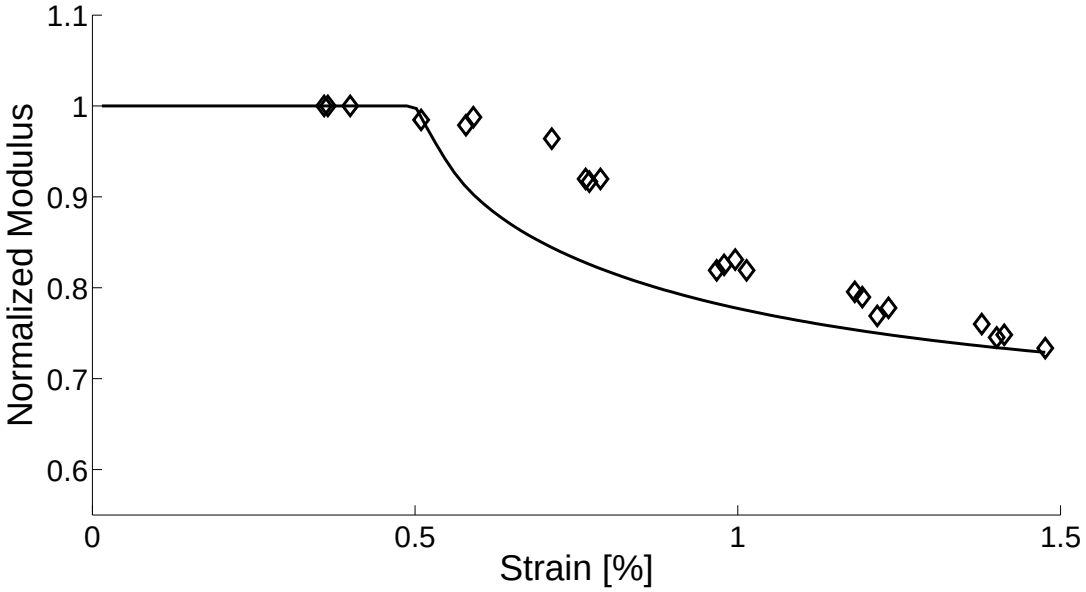

Figure 4: Comparison between predicted and experimental values of modulus vs. applied strain for $[0_2/90_4]_S$.

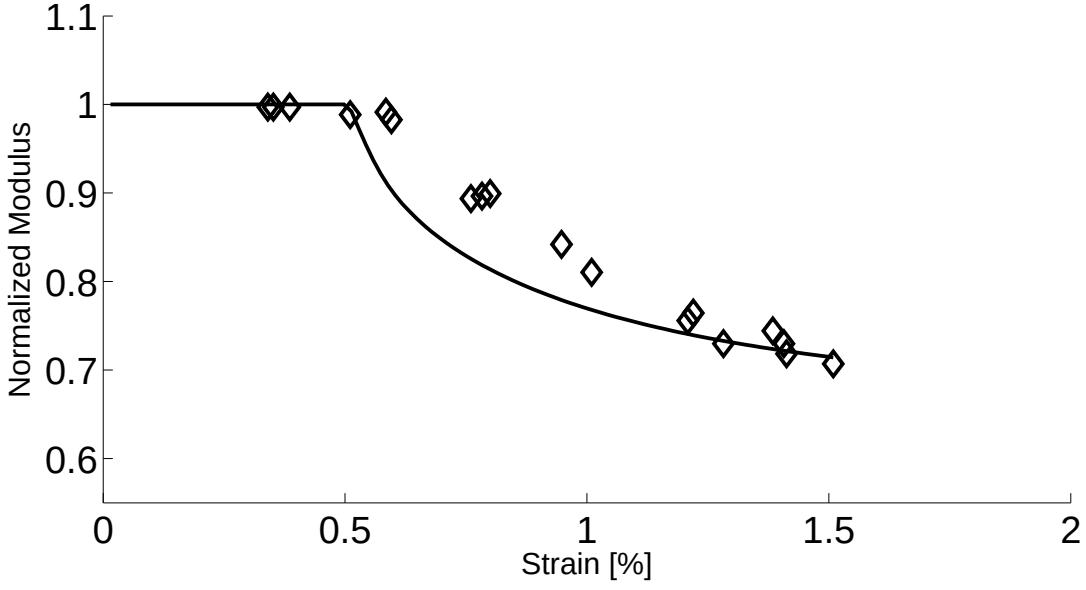

Figure 5: Comparison between predicted and experimental values of modulus vs. applied strain for $[\pm 15/90_4]_S$.

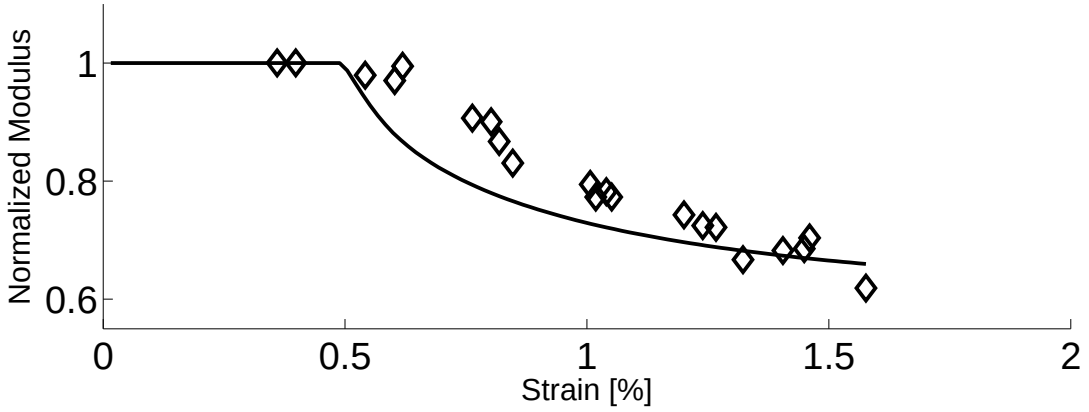

Figure 6: Comparison between predicted and experimental values of modulus vs. applied strain for $[\pm 30/90_4]_S$.

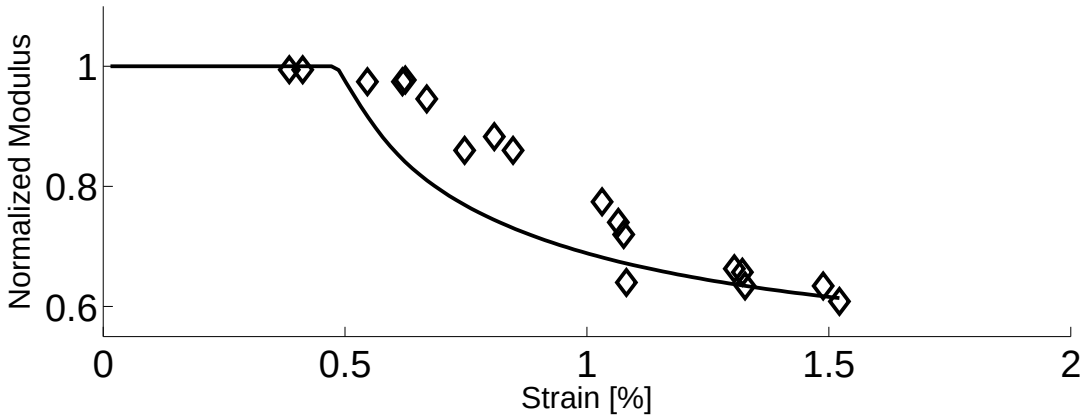

Figure 7: Comparison between predicted and experimental values of modulus vs. applied strain for $[\pm 40/90_4]_S$.

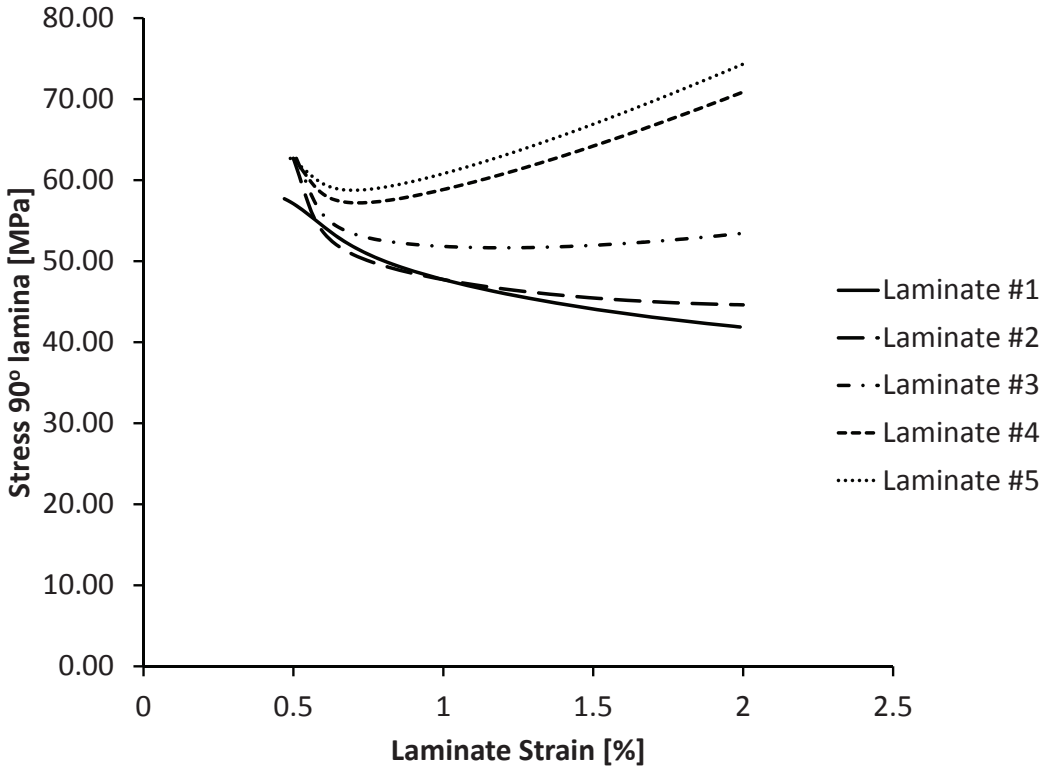

Figure 8: Stress vs. strain in the cracking lamina.

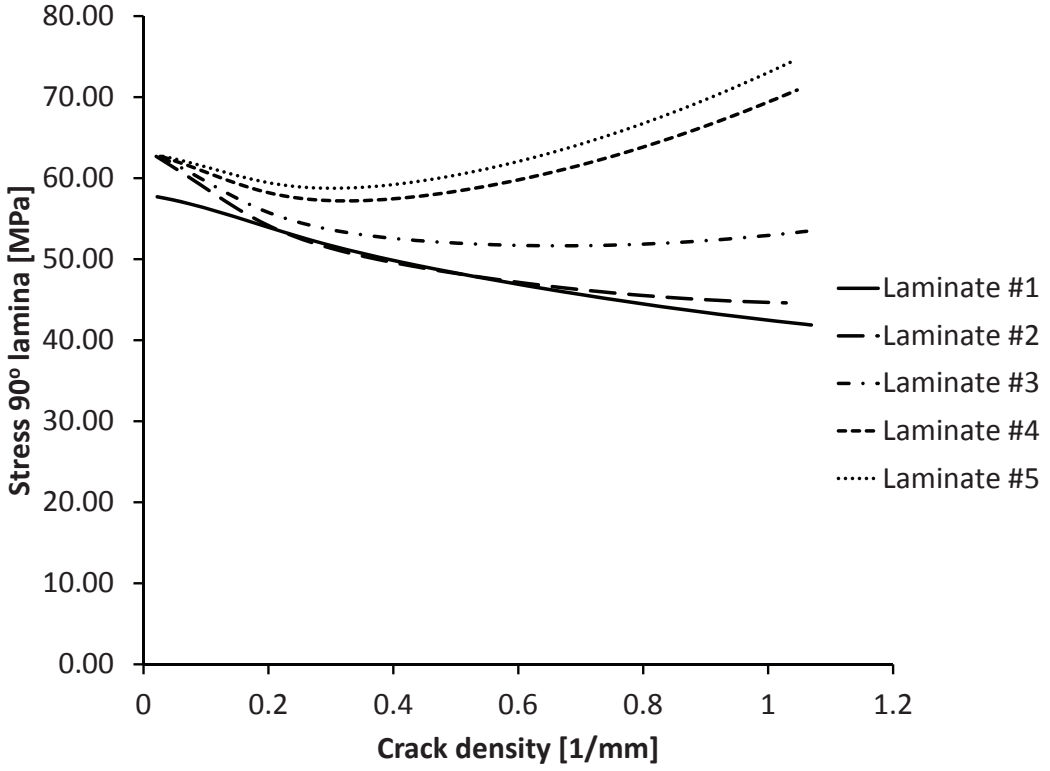

Figure 9: Stress vs. crack density in the cracking lamina.

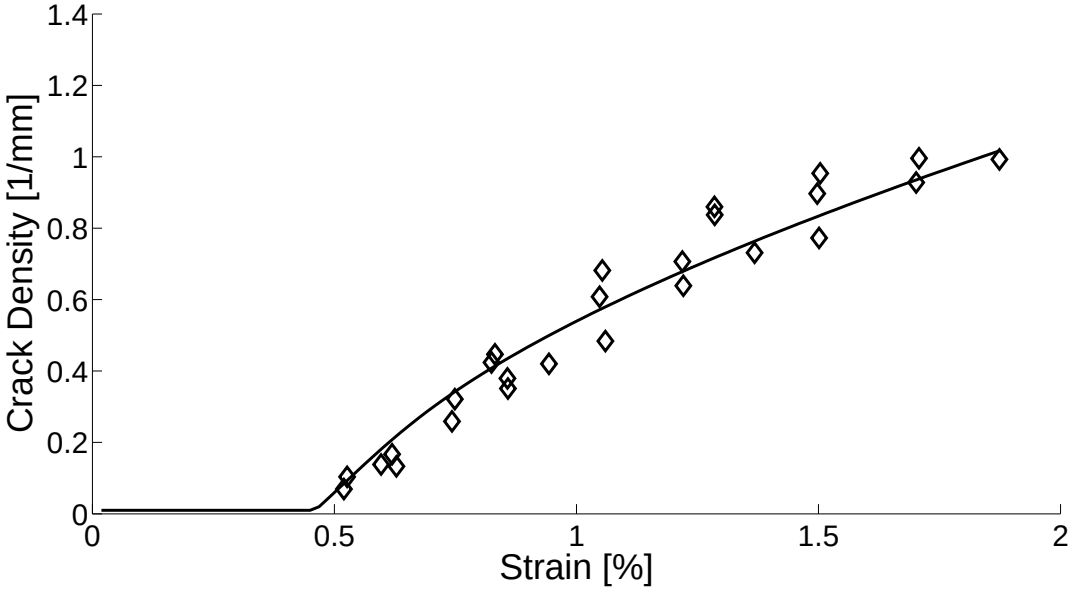

Figure 10: Identification of G_{IC} using experimental data for $[0/90_8/0_{1/2}]_S$.

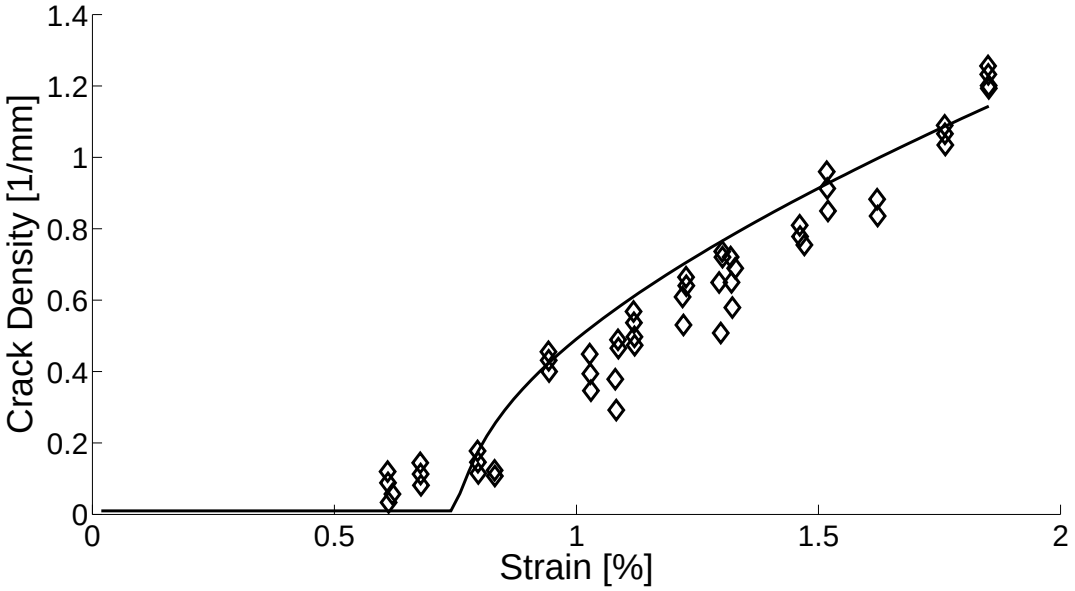

Figure 11: Comparison between predicted and experimental values of crack density vs. applied strain for $[0 \pm 70_4/0_{1/2}]_S$.

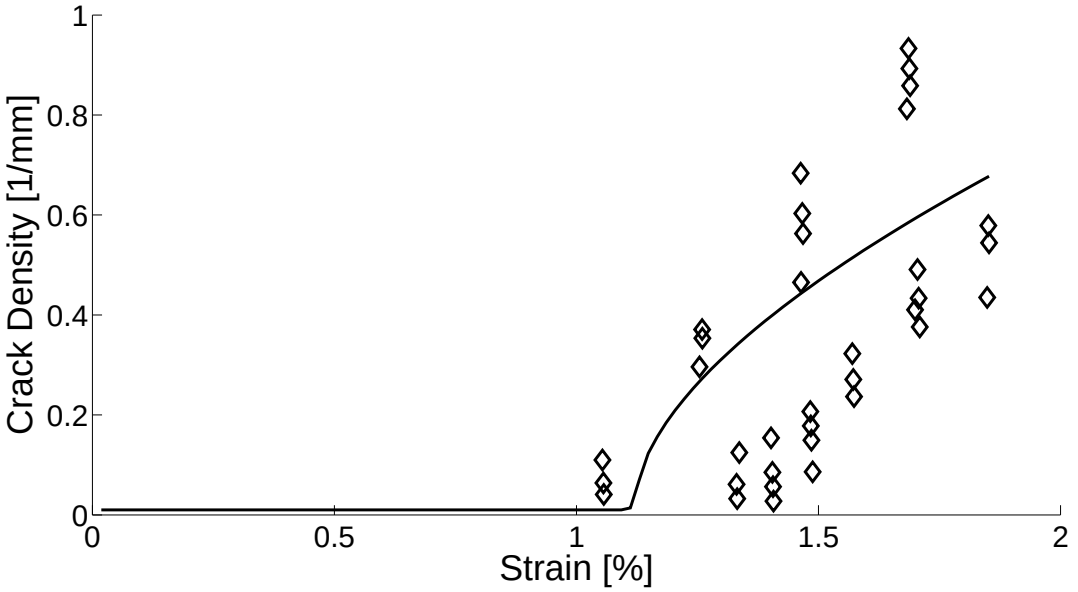

Figure 12: Comparison between predicted and experimental values of crack density vs. applied strain for $[0 \pm 55_4/0_{1/2}]_S$

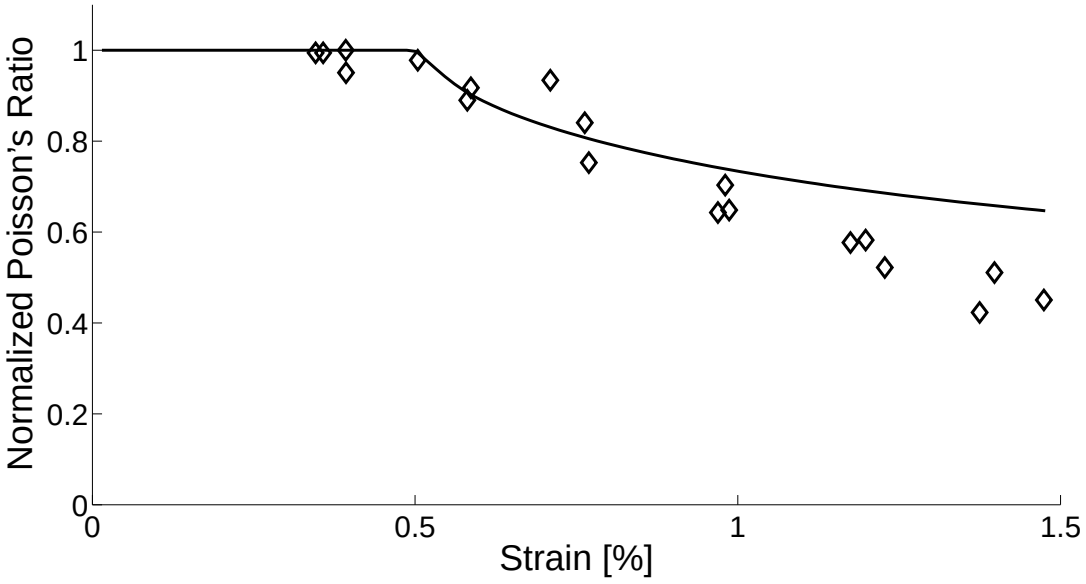

Figure 13: Comparison between predicted and experimental values of Poisson's ratio vs. applied strain for $[0_2/90_4]_S$.

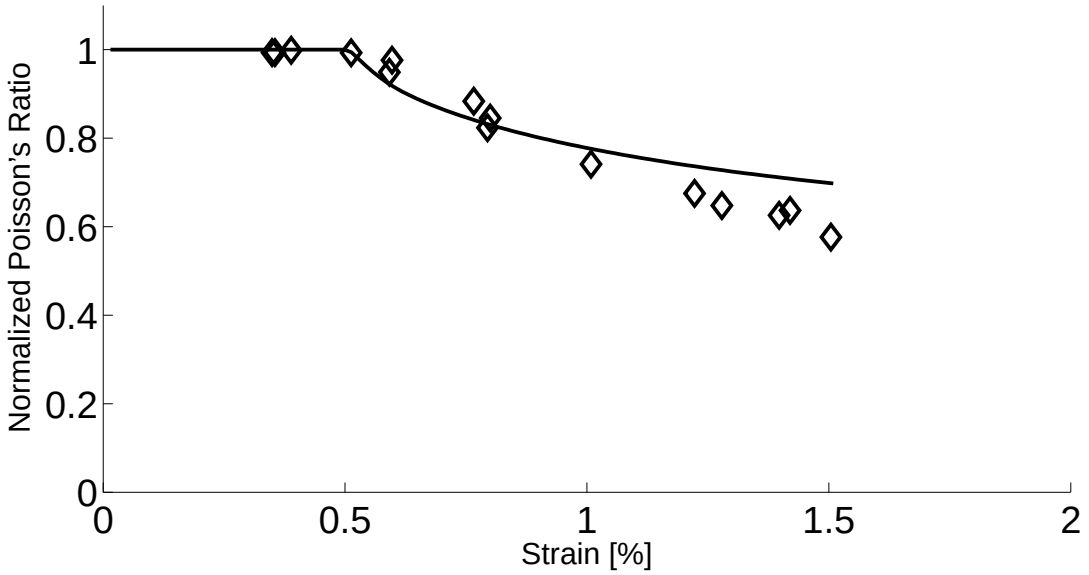

Figure 14: Comparison between predicted and experimental values of Poisson's ratio vs. applied strain for $[\pm 15/90_4]_S$.

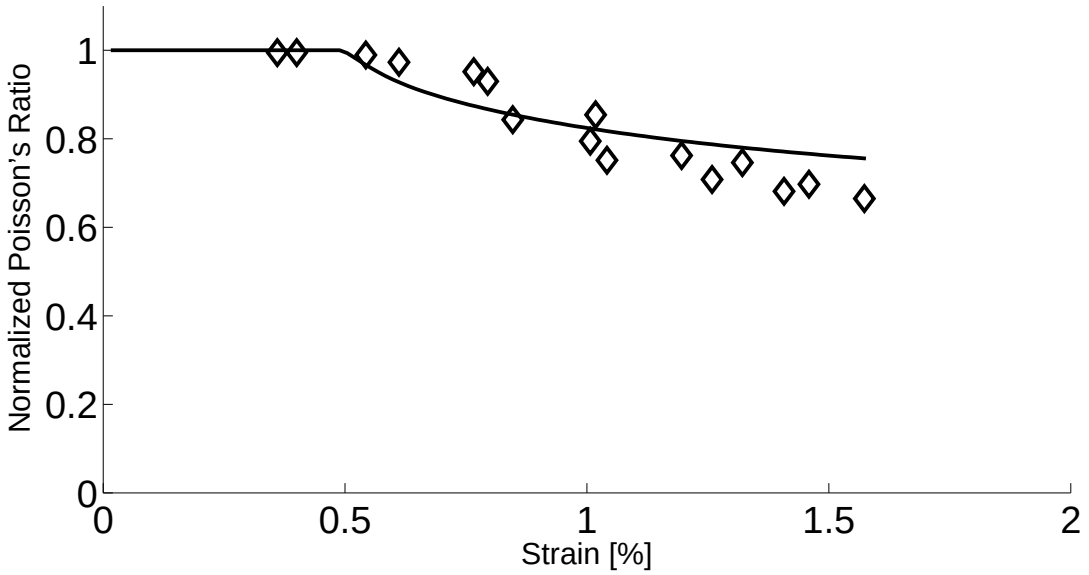

Figure 15: Comparison between predicted and experimental values of Poisson's ratio vs. applied strain for $[\pm 30/90_4]_S$.

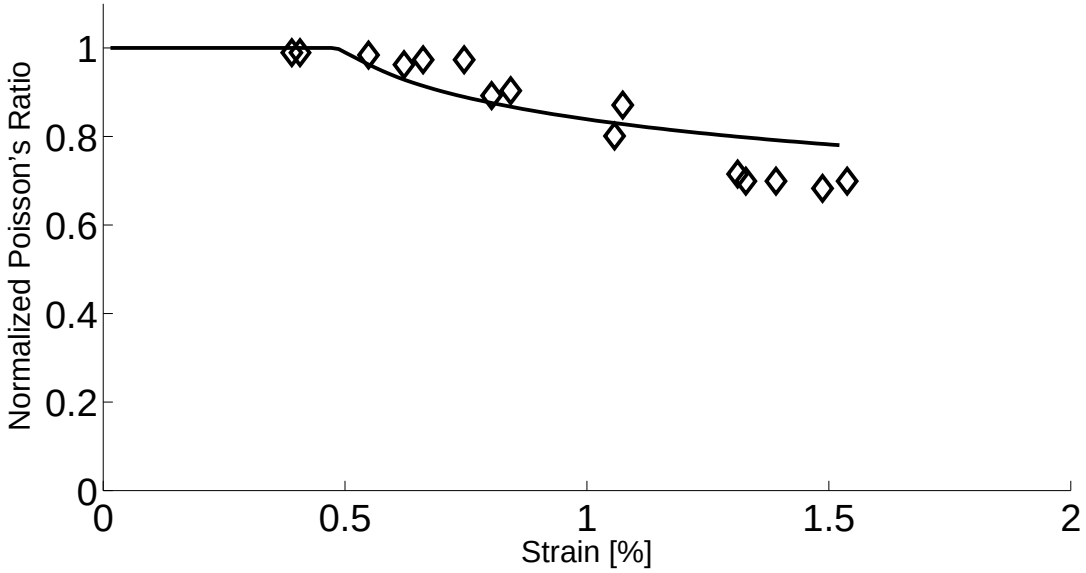

Figure 16: Comparison between predicted and experimental values of Poisson's ratio vs. applied strain for $[\pm 40/90_4]_S$.

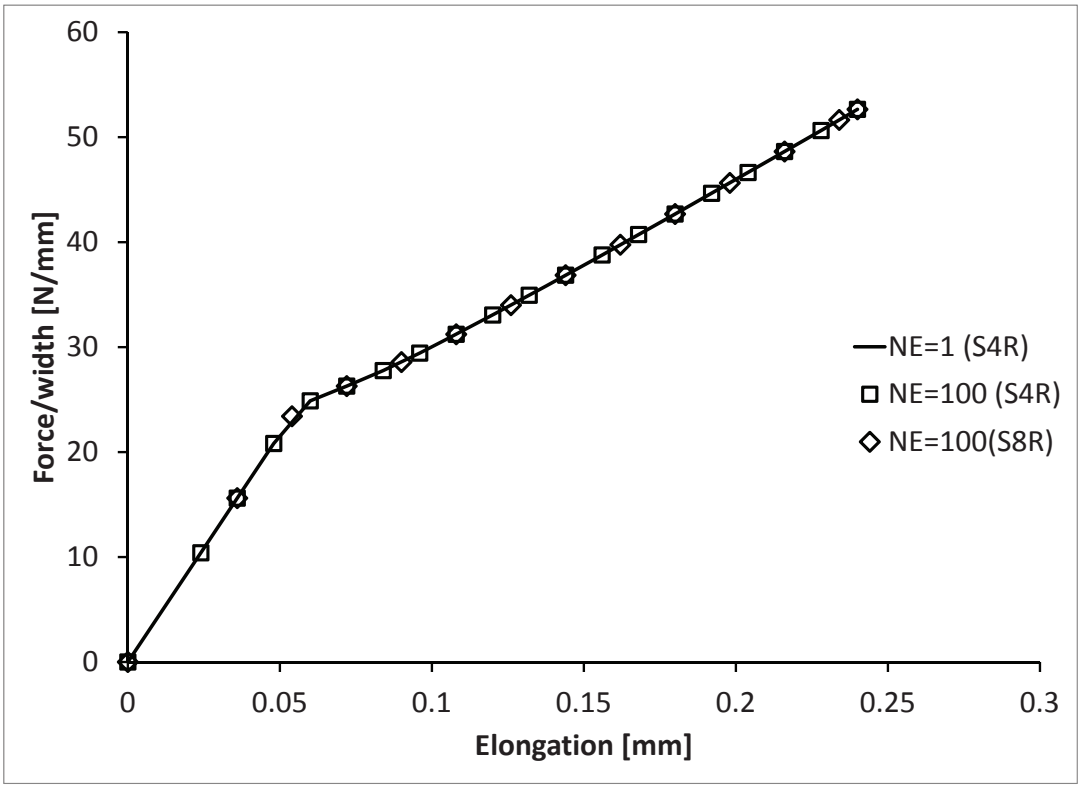

Figure 17: Objectivity of the model. The predictions are independent of element size and type.

Tables

Table 1: Laminate description.

Lam. Num.	LSS	t [mm]	Ex [Mpa]	ϵ FPF [$\mu\epsilon$]	Ref.
cracks in 90° laminas with 0° supporting					
1	$[0/90_8/0_1/2]_S$	2.74	17841	5000	[44, Fig. 1]
2	$[0_2/90_4]_S$	1.73	23539	5900	[42, Fig. 7]
cracks in 90° laminas with $\pm\theta$° supporting					
3	$[\pm 15/90_4]_S$	1.73	22087	5800	[42, Fig. 8]
4	$[\pm 30/90_4]_S$	1.73	18608	6200	[42, Fig. 9]
5	$[\pm 40/90_4]_S$	1.73	16179	6700	[42, Fig. 10]
cracks in $\pm\theta$° laminas					
6	$[0/\pm 70_4/0_1/2]_S$	2.74	17879	6100	[44, Fig. 2]
7	$[0/\pm 55_4/0_1/2]_S$	2.74	18995	10500	[44, Fig. 3]

Table 2: In-situ strength calculations.

Lam. Num. -	FPF exp [N/mm]	FPF CLT [N/mm]	FPF in-situ [N/mm]	% error w/in-situ	% error w/o in-situ	F2T corrected [MPa]
1	244	154	244	0	-58	40
2	240	129	204	-17	-86	47
3	221	122	193	-15	-82	46
4	199	104	164	-22	-93	49
5	187	90	143	-31	-108	52
6	298	171	316	6	-75	38
7	546	229	413	-32	-138	53
Average				16	91	46.38

References

[1] E. J. Barbero. Prediction of compression strength of unidirectional polymer matrix composites. *Journal of Composite Materials*, 32(5)(5):483–502, 1998.

[2] A. Puck and H. Schürmann Failure analysis of FRP laminates by means of physically based phenomenological models *Composites Science and Technology*, 62:1633–1662, 2002.

[3] C. Davila and P. Camanho. Failure Criteria for FRP Laminates in Plane Stress. *NASA/TM-2003-212663*, pages 1–28, 2003.

[4] E. J. Barbero. *Introduction to Composite Materials Design–Second Edition.* CRC Press, Boca Raton, FL, 2nd edition, 2010.

[5] P. Ladevèze, O. Allix, J.F. Deü and D. Lévêque A mesomodel for localisation and damage computation in laminates *Computer Methods in Applied Mechanics and Engineering*, 183(1-2):105–122, 2000.

[6] P. Ladevèze, O. Allix, B. Douchin and D. Lévêque A computational method for damage intensity prediction in a laminated composite structure *Computational Mechanics. New Trends and Applications*, Editor S. Idelsohn, E. Oñate and E. Dvorkin. CIMNE, Barcelona, 1998.

[7] P. Ladevèze A Damage Mesomodel of Laminate Composites Chapter in *Handbook of Materials Behavior Models: Nonlinear Models and Properties*, pages 1004–1014. Editor J. Lemaitre. Academic Press, 2001.

[8] E. Abisset, F. Daghia and P. Ladevèze On the validation of a damage mesomodel for laminated composites by means of open-hole tensile tests on quasi-isotropic laminates *Composites Part A: Applied Science and Manufacturing*, 42(10):1515–1524, 2011.

[9] F. Rastellini, S. Oller, O. Salomón, E. Oñate Composite materials non-linear modelling for long fibre-reinforced laminates: Continuum basis, computational aspects and validations. *Computers & Structures*, 86(9):879–896, 2008

[10] X. Martinez, S. Oller and E. Barbero Study of delamination in composites by using the serial/parallel mixing theroy and a damage formulation. Chapter in *Mechanical response of composites*, pages 119–140. Editor P Camanho. Springer, 2008.

[11] X. Martinez and S. Oller Numerical simulation of matrix reinforced composite materials subjected to compression loads. *Archives of computational methods in engineering*, 16(4):357–397, 2009.

[12] X. Martinez, F. Rastellini, S. Oller, F. Flores and E. Oñate Computationally optimized formulation for the simulation of composite materials and delamination failures. *Composites Part B: Engineering*, 42(2): 134–144, 2011.

[13] R. J. Nuismer and S. C. Tan. Constitutive relations of a cracked composite lamina. *Journal of Composite Materials*, 22:306–321, 1988.

[14] S. C. Tan and R. J. Nuismer. A theory for progressive matrix cracking in composite laminates. *Journal of Composite Materials*, 23:1029–1047, 1989.

[15] S. Li, S. R. Reid, and P. D. Soden. A continuum damage model for transverse matrix cracking in laminated fibre-reinforced composites. *Philosophical Transactions of the Royal Society London, Series A (Mathematical, Physical and Engineering Sciences)*, 356:2379–2412, 1998.

[16] E. Adolfsson and P. Gudmundson. Matrix crack initiation and progression in composite laminates subjected to bending and extension. *International Journal of Solids and Structures*, 36:3131–3169, 1999.

[17] J. A. Nairn. *Polymer Matrix Composites*, volume 2 of *Comprehensive Composite Materials*, chapter Matrix Microcracking in Composites, pages 403–432. Elsevier Science, 2000.

[18] J. M Berthelot. Transverse cracking and delamination in cross-ply glass-fiber and carbon-fiber reinforced plastic laminates: static and fatigue loading. *Applied Mechanics Review*, 56:111–147, 2003.

[19] J. A. Nairn. *Finite Fracture Mechanics of Matrix Microcracking in Composites*, pages 207–212. Application of Fracture Mechanics to Polymers, Adhesives and Composites. Elsevier, 2004.

[20] S. H. Lim and S. Li. Energy release rates for transverse cracking and delaminations induced by transverse cracks in laminated composites. *Composites Part A*, 36(11):1467–1476, 2005.

[21] D. T. G. Katerelos, J. Varna, and C. Galiotis. Energy criterion for modeling damage evolution in cross-ply composite laminates. *Composites Science and Technology*, 68:2318–24, 2008.

[22] D. T. G. Katerelos, M. Kashtalyan, C. Soutis, and C. Galiotis. Matrix cracking in polymeric composites laminates: Modeling and experiments. *Composites Science and Technology*, 68:2310–17, 2008.

[23] A. Adumitroaie, and E. J. Barbero, Intralaminar Damage Model for Laminates Subjected to Membrane and Flexural Deformations, *Mechanics of Advanced Materials and Structures,* http://dx.doi.org/10.1080/15376494.2013.796541

[24] A. Matzenmiller, J. Lubliner, and R. Taylor. A constitutive model for anisotropic damage in fiber-composites. *Mechanics of Materials*, 20:125–152, 1995.

[25] P. Camanho and C. Davila. Mixed-mode decohesion finite elements for the simulation of delamination in composite materials. *NASA/TM-2002-211737*, pages 1–37, 2002.

[26] Simulia. Abaqus analysis user's manual, version 6.12, section 24.3.

[27] GENOA Virtual Testing & Analysis Software, Alpha STAR Corporation, http://www.ascgenoa.com.

[28] Helius:MCT Composite Materials Analysis Software, Firehole Composites, http://www.firehole.com/products/mct/.

[29] E. J. Barbero. Finite Element Analysis of Composite Materials using Abaqus. Web resource: http://barbero.cadec-online.com/feacm-abaqus.

[30] E. J. Barbero. Finite Element Analysis of Composite Materials using ANSYS. Web resource: http://barbero.cadec-online.com/feacm-ansys.

[31] E. Barbero and D. Cortes. A mechanistic model for transverse damage initiation, evolution, and stiffness reduction in laminated composites. *Composites Part B*, 41:124–132, 2010.

[32] J. Oliver. A consistent characteristic length for smeared cracking models. *International Journal for Numerical Methods in Engineering*, 28(2):461–74, 02 1989.

[33] E. J. Barbero and L. De Vivo. Constitutive model for elastic damage in fiber-reinforced pmc laminae. *International Journal of Damage Mechanics*, 10(1):73–93, 2001.

[34] E. J. Barbero, F. A. Cosso, R. Roman, and T. L. Weadon. Determination of material parameters for Abaqus progressive damage analysis of E-Glass Epoxy laminates, http://dx.doi.org/10.1016/j.compositesb.2012.09.069. *Composites Part B:Engineering*, 46(3):211–220, 2012.

[35] ANSYS Inc. Ansys mechanical apdl programmer's manual, release 14.0, 2011.

[36] Computer Aided Design Environment for Composites (CADEC) http://en.cadec-online.com.

[37] P. Davies. *Protocols for Interlaminar Fracture Testing of Composites*. Polymer and Composites Task Group. European Structural Integrity Society (ESIS), Plouzané, France, 1992.

[38] R. Rikards, F.G. Buchholz, H. Wang, A.K. Bledzki, A. Korjakin, and H.A. Richard. Investigation of mixed mode i/ii interlaminar fracture toughness of laminated composites by using a cts type specimen. *Engineering Fracture Mechanics*, 61:325–342, 1998.

[39] T. Yokozeki, T. Aoki, and T. Ishikawa. Transverse crack propagation in the specimen width direction of cfrp laminates under static tensile loadings. *Journal of Composite Materials*, 36(17):2085–99, 2002.

[40] E. J. Barbero. *Finite Element Analysis of Composite Materials Using Abaqus*. CRC Press, 2013.

[41] E. J. Barbero. *Finite Element Analysis of Composite Materials Using ANSYS-Second Edition*. CRC Press, 2014.

[42] J. Varna, R. Joffe, and R. Talreja. A synergistic damage mechanics analysis of transverse cracking in $[\pm\theta/90_4]_s$ laminates. *Composites Science and Technology*, 61:657–665, 2001.

[43] E. J. Barbero. *Finite Element Analysis of Composite Materials*. Taylor & Francis, 2007.

[44] J. Varna, R. Joffe, N. Akshantala, and R. Talreja. Damage in composite laminates with off-axis plies. *Composites Science and Technology*, 59:2139–2147, 1999.

[45] A. S. D. Wang. Fracture mechanics of sublaminate cracks in composite materials. *Compos. Tech. Review*, 6:45–62, 1984.

[46] E. J. Barbero and F. A. Cosso. Determination of Material Parameters for Discrete Damage Mechanics Analysis of Carbon-Epoxy Laminates. *Composites Part B*, 56:638–646, 2014. http://dx.doi.org/10.1016/j.compositesb.2013.08.084

[47] J. Lagarias, J. Reeds, M. Wright, and P. Wright. Convergence properties of the nelder-mead simplex method in low dimensions. *SIAM Journal of Optimization*, 9:112–147, 1998.